

Article

Effect of a Healing Agent on the Curing Reaction Kinetics and Its Mechanism in a Self-Healing System

Xianfeng Wang ¹, Ming Zhang ^{2,*}, Feng Xing ^{1,*} and Ningxu Han ¹

¹ Guangdong Provincial Key Laboratory of Durability for Marine Civil Engineering, College of Civil Engineering, Shenzhen University, Shenzhen 518060, China; xfw@szu.edu.cn (X.W.); nxhan@szu.edu.cn (N.H.)

² College of Civil Science and Engineering, Yangzhou University, Yangzhou 225127, Jiangsu, China

* Correspondence: zhangmingjob@sina.com (M.Z.); xingf@szu.edu.cn (F.X.); Tel.: +86-514-8797-9409 (M.Z.)

Received: 7 October 2018; Accepted: 7 November 2018; Published: 14 November 2018



Featured Application: Microcapsule based self-healing system is developed for intelligent repair of microcracks or/and damage in cementitious composites.

Abstract: Self-healing cementitious composites have been developed by using microcapsules. In this study, the effect of the healing agent on the crosslinking and curing reaction kinetics was analyzed. The effect of the diluent n-butyl glycidyl ether (BGE) on the reaction was investigated for five fractions, namely 10.0%, 12.5%, 15.0%, 17.5%, and 20.0% mass fractions to epoxy resin. The Kissinger and Crane equations were used to obtain the activation energy and reaction order with different mass fractions of diluent, as well as the kinetic parameters of the curing reaction. The optimal fraction of BGE was determined as 17.5%. Likewise, the effect of the curing agent MC120D on the reaction kinetics was investigated for 10%, 20%, 30%, 40%, and 50% mass fractions to the diluted epoxy resin. The optimal fraction was determined as 20%. The mechanism of the curing reaction with the healing agent was investigated. The infrared spectra of the cured products of 20% MC120D with BGE/E51 (0.0%, 12.5%, 15.0%, 20.0%, 100%) were analyzed. It is shown that not only the epoxy resin E-51 was cured, but also that the BGE was involved in the cross-linking reaction of the epoxy resin E-51 with MC120D.

Keywords: microcapsules; self-healing; curing reaction; n-butyl glycidyl ether (BGE); MC120D

1. Introduction

Based on the principle of bionics, the intelligent integrated concrete materials and structures with self-healing ability are prepared. They can automatically locate and repair the micro-damaged parts in the concrete structure and improve the performance of the concrete materials. Bionic self-healing of concrete material refers to imitating the damage healing function of biological tissue, whereby the special components that are embedded in the cementitious matrix form an intelligent self-healing system. When cracks initiate due to damage, the healing system that is embedded in the matrix is triggered by the force, heat, or chemical damage and releases a healing agent to bond the cracks and prevent further extension of the crack, with the purpose of achieving the repair. When compared with the traditional repair technology, a self-healing system has the advantages of low cost, no need to rely on external operations, good renewability, etc. For self-healing, a relatively rapid response is required to reconstruct the structural integrity or to prevent to a certain extent further propagation of the crack [1–7].

In recent years, various studies have been conducted using microcapsule technology to achieve self-healing functionality in cementitious materials [8–16]. Su et al. [17–19] fabricated microcapsules using rejuvenator diphenylsilane (DPS) as the core material and analyzed the diffusion behavior

of microencapsulated rejuvenator in aged bitumen by Fourier-transform infrared spectroscopy (FTIR). They also investigated the self-healing performance of bitumen by a modified fracture healing–refracture method through a repetitive tension test using microcapsules containing rejuvenator. Later, they employed a modified beam on elastic foundation (BOEF) method to investigate the mechanical properties of bitumen/microcapsule materials, in which microcapsules of different sizes and shell thickness were evaluated. Lv and Schlangen et al. [20,21] developed a type of polymeric microcapsule for the self-healing of microcracks in cementitious materials, while using phenol–formaldehyde resin for the shell and dicyclopentadiene as the healing agent. They examined and analyzed the rupture behavior and crack surface of cement paste with embedded microcapsules by X-ray computed tomography (XCT). In addition, the chemical stability of the microcapsules and the trigger performance were verified in a simulated concrete pore solution and hardened cement paste specimens. Additionally, the relationship between the physical properties of the microcapsules and their micromechanical properties were investigated using nanoindentation. They found that the mechanical force that is required to trigger the self-healing function of microcapsules increased with the increase of the mean size of microcapsules and the decrease of shell thickness.

De Belie’s group [22–24] used encapsulated bacterial spores for self-healing concrete. They investigated the applicability of encapsulated spores and the influence of microcapsules on mortar specimens. The crack healing ratio and the water permeability were evaluated to determine the self-healing capacity. They also studied the microstructure of the capsules containing self-healing materials by micro-computed tomography analysis. The results of this analysis revealed the three-dimensional distribution and de-bonding of the microcapsules in their native state in a polymer system with self-healing properties. They also studied the rupturing capability of microcapsules when crossed by a crack in concrete of a typical size. The suitability of five types of polymeric capsules was assessed by using a numerical model to screen the best performing capsules and verifying their suitability by experimental methods. Capsules that were made of a specific type of poly(methyl methacrylate) (PMMA) were evaluated. They determined that thick walls were unsuitable as the microcapsules ruptured for larger crack sizes.

Since 2008, attempts have been made to introduce a novel microcapsule-based self-healing system for concrete at Guangdong Provincial Key Laboratory of Durability for Marine Civil Engineering, Shenzhen University [8–15]. The urea formaldehyde resin was used for the wall of the microcapsule, and bisphenol—an epoxy resin E-51 diluted with n-butyl glycidyl ether (BGE)—was adopted as the healing-agent inside the microcapsule. MC120D, a latent curing agent, was used for curing the healing product. The results showed that the microcapsule that was obtained with the adopted production process could be used for the self-healing system in concrete. The self-healing performance of the cementitious materials in mechanical strength, permeability, and microstructures was investigated. Additionally, the interaction between the crack and the microcapsule was studied by numerical analysis using the parameters of location of the crack, microcapsule shell thickness, strength of the microcapsule shell, and the debonding strength of the interface between microcapsule and mortar matrix. Also, a criterion was derived to judge the rupture or debonding of the microcapsule.

However, the mechanism of self-healing process based on microcapsules has not been fully investigated. The objective of this study is to analyze the curing kinetics of different mass fractions of the diluent BGE and the curing agent MC120D by differential thermal analysis based on Kissinger’s equation and Arrhenius’ equation. The optimal amount of the BGE diluent and the curing agent was determined at the lowest activation energy and reaction rate. The cured products were analyzed by FTIR spectroscopy. The mechanism of appearance and disappearance of the exothermic peaks was determined.

2. Materials and Methods

2.1. Materials

As mentioned above, the developed self-healing concrete is based on organic microcapsules. For the core material, in this study, bisphenol A type epoxy resin E-51 (Shenzhen Yoshida Chemical Co., Ltd., Shenzhen, China) was adopted for the microcapsule component materials due to its high bond strength, wide adhesion, good stability, low shrinkage of curing products, and good mechanical properties [25]. However, due to its viscosity at room temperature, epoxy resin E-51 is not conducive to the siphon phenomenon when microcapsules rupture in the matrix. Accordingly, it is necessary to add a diluent to reduce the viscosity of the resin E-51, so that the resin glue is more prone to infiltrate the surface of the crack wall and have good compatibility with the epoxy resin E-51. BGE (Shanghai Bangcheng Chemical Co., Ltd., Shanghai, China) is a liquid at room temperature, and its viscosity is very low. Due to the molecular structure of the ether bond and epoxy bond, it can participate in the curing reaction of epoxy resin, therefore BGE was adopted as an active diluent for the epoxy resin.

BGE was added to the epoxy resin at different mass fractions, and the viscosity was measured after mixing at room temperature (26 °C) (Figure 1). When the content of BGE was 0~10%, the viscosity of E-51 decreased sharply with the increase of the BGE content. When the content of BGE was 10~20%, the viscosity of E-51 decreased slowly. When the BGE content was greater than 20%, the E-51 viscosity no longer changed. This is because E-51 is an oligomer, which has hydrogen bonds and other active groups on the molecular chain, thus the intermolecular force is relatively strong. The diluent may play a role in the dispersion of E-51 when present at a certain dosage range, at which the intermolecular force is decreased. However, if the diluent content exceeds a certain level, this effect is no longer obvious. The results that are shown in Figure 1 reveal that the suitable content of BGE is between 10 to 20%. The specific content of epoxy resin may be determined through analysis of the curing kinetics.

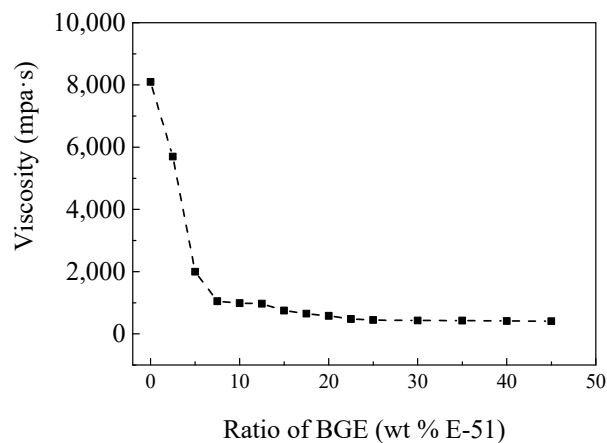


Figure 1. Effect of the n-butyl glycidyl ether (BGE) diluent on the viscosity of epoxy E-51.

For the wall material, as the urea-formaldehyde resin has good mechanical properties, heat resistance, and tightness, water can also be used as a dispersion medium to synthesize the wall material by the solution polymerization method, in this study, urea-formaldehyde resin was used as the wall of microcapsules.

The epoxy resin as the core material can be converted into a three-dimensional mesh structure only by adding a curing agent. In order to ensure the self-healing effect, the latent curing agent MC120D was selected for this study.

In the test for the healing agent, the content of MC120D was fixed at 20% of the diluted epoxy resin, and the mass fraction of BGE to epoxy resin was fixed at 10.0%, 12.5%, 15.0%, 17.5%, and 20.0%. After mixing, the mixture was sealed and allowed to stand for one day for the test.

2.2. Theoretical Basis

The curing process of the epoxy resin-curing agent system follows the Arrhenius equation [26], expressed as:

$$d\alpha/dt = Ae^{-E/RT}(1-\alpha)^n, \quad (1)$$

where $d\alpha/dt$ is the curing reaction rate; α denotes the curing degree (%); t is the curing time (min); A represents the pre-exponential factor (1/s); E denotes the activation energy for the reaction (J/mol); R is the universal gas constant (8.31 J/K·mol); T is the absolute temperature in the reaction (K); and, n denotes the reaction order constant.

When the temperature increases during the curing process, the cure rate $d\alpha/dt$ will reach its maximum value and then decrease to zero as the reactants are depleted, and when $d(d\alpha/dt)/dt$ is zero, the maximum value is reached. If the temperature rises at a constant rate, $\beta = dT/dt$ [27], Arrhenius equation becomes the Kissinger equation [28], expressed as:

$$d\left(\ln \frac{\beta}{T_p^2}\right)/d\left(\frac{1}{T}\right) = -\frac{E}{R}, \quad (2)$$

where T_p is the peak temperature. When $E/nR \gg 2T_p$, Crane equation [29] is obtained:

$$\frac{d(\ln \beta)}{d(1/T_p)} \approx -\frac{E}{nR}, \quad (3)$$

The E of the curing reaction is a quantitative parameter for measuring the activity of the curing reaction of each system. It is the summation of the activation energies of the various reactions during the curing. On one hand, according to the Kissinger equation, the values of $-\ln(\beta/T_p^2)$ and $1000/T_p$ are calculated based on the differential scanning calorimetry (DSC) data. The activation energy E for the curing reaction can be obtained from the slope of the regression line after plotting the data of $-\ln(\beta/T_p^2)$ and $1000/T_p$. On the other hand, according to the Crane equation, the values of $-\ln\beta$ and $1000/T_p$ are calculated based on the DSC data. The reaction order constant can be obtained from the slope of the regression line after plotting the data of $-\ln\beta$ and $1000/T_p$. The activation energy of the curing reaction reflects the degree of difficulty in the reaction and the higher the activation energy, the more energy is required in the curing reaction.

From the Kissinger equation and the Arrhenius equation, the frequency factor A (1/s) and the rate constant k [30] can be obtained, as follows:

$$A = \frac{\beta E \exp(E/RT_p)}{RT_p^2}, \quad (4)$$

$$k = A \exp(-E/RT_p), \quad (5)$$

Here, the frequency factor A is a measure of the degree of chaos before and after the reaction, and the rate constant k indicates the degree of reaction at the peak temperature.

2.3. Experimental Methods

2.3.1. Kinetic Analysis of the Curing Reaction

In this study, the kinetic analysis was conducted using an integrated Thermo-Gravimetric/Differential Thermal Analyzer NETZSCH STA 409 PC (NETZSCH GABO Instruments GmbH, Selb, Germany). As the experiment involved the use of a healing agent containing volatile liquid, the test results may be greatly affected by the instrument internal air humidity and the stability of the instrument. To address this issue, the test process was conducted, as follows: the instrument was switched on and run 1 d before the experiment, and the source of high purity nitrogen (used both as purge and protective gas) was turned on. Before testing, the instrument was run with a baseline temperature program, using a heating rate of 10 K/min, a peak temperature of 1000 °C, and a reset temperature of 1010 °C.

After the analyzer finished running the baseline program, the instrument was run twice with the baseline program without samples, so that the moisture in the furnace was completely removed and the instrument was in stable working condition. Then, the test program was conducted up to temperature of 500 °C using heating rates of 5, 10, 15, and 20 K/min.

The basic steps for the sample test were as follows. First, the reference crucible and the testing crucible were placed on the stent. After closing the furnace, the crucible mass was cleared on the software and then the test sample was placed in the furnace and the instrument was run with the appropriate program. In order to prevent the volatiles of the healing agent from adhering to the furnace or exhaust channel, after testing of 3–5 samples, the instrument was run without samples at a peak temperature of 1000 °C, so that the cured material that may have adhered onto the furnace and the exhaust passage was completely volatilized.

It can be seen that the test temperature was much high, although the application background is usually at room temperature. This is because the test program was used to determine the kinetic parameters for the curing reaction. The mechanism of the curing reaction is also analyzed. In reality, the situation of conflagration may cause temperature rising to a high level.

2.3.2. Fourier Transform Infrared (FTIR) Analysis

The epoxy resin cured product was analyzed by FTIR spectroscopy. To ensure the full reaction at each stage, the maximum curing temperature was set at 170 °C and 270 °C, with a heating rate of 10 °C/min. When the set temperature was reached, it was held for 30 min, and then cooled naturally to room temperature. After grinding, the infrared (IR) spectrum of the cured product was obtained using a Perkin-Elmer Spectrum BXII spectrometer (Perkin Elmer Inc., Shelton, CT, USA). For the FTIR analysis of the cured products of the healing agent, first, 200 mg of KBr and 2 mg of the cured product were mixed together and ground. Then, the ground sample was placed in a compressed sheet mold and pressed into a transparent sample pellet with a uniform thickness. The sample was mounted on the instrument, analyzed in the range of 4000 to 400 cm^{-1} , and the transmittance from 0 to 100 T%. For the FTIR analysis of the healing agent glue, a KBr pellet was prepared, and then the sample was dropped onto the KBr pellet, so that the pellet surface was just completely infiltrated. Next, the pellet was placed on the instrument. The subsequent process was the same as that for the cured product.

3. Results and Discussion

3.1. Effect of the BGE Diluent on Reaction Kinetics

The differential thermal curves of the epoxy diluted with BGE at 12.5%, 15%, 17.5%, and 20%, are shown in Figure 2 at different heating rate. The curves reveal that the healing agent has two major exothermic peaks, and the first exothermic peak is significantly sharper than the second one. This indicates that the curing reaction occurred in two stages [31,32], and the reaction rate in the first stage was greater than that in the second stage. With the increase of the heating rate, the initial

temperature (T_i), peak temperature (T_p), and the termination temperature (T_f) of the system shifted in the direction of the high temperature. However, the higher the heating rate, the broader the exothermic peak. The heat is more concentrated at the low heating rate.

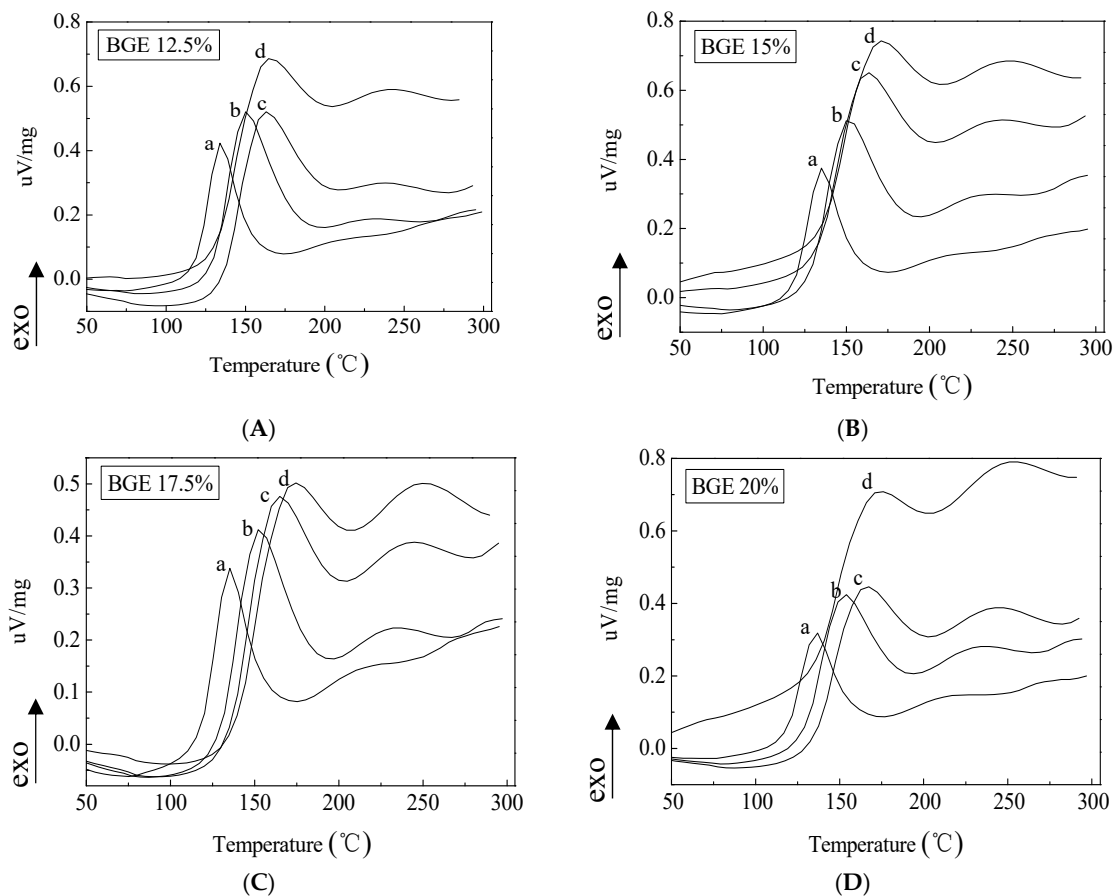


Figure 2. Differential thermal analysis of the healing system with different mass fractions of BGE (a. 5 K/min, b. 10 K/min, c. 15 K/min, d. 20 K/min). (A) 12.5% BGE; (B) 15% BGE; (C) 17.5% BGE; and, (D) 20% BGE.

The values $-\ln(\beta/T_p^2)$ are plotted against $1000/T_p$ in Figure 3A according to the temperature of the first peak of the curing reaction at different heating rates, and they show a good linear relationship. This indicates that it should be reasonable to study the kinetics of the above system while using the Kissinger equation (Equation (2)). The activation energy E of the curing reaction was calculated from the slope of the regression straight line according to Equation (2). In the same manner, the plotting of $-\ln\beta$ against $1000/T_p$ (Figure 3B) also shows a good linear relationship. Accordingly, it is feasible to use the Crane equation to study the kinetics of the system. The order of the curing reaction can be calculated from the slope and activation energy.

The activation energy and reaction order with different BGE mass fractions shown in Table 1 reveal that a BGE content of 17.5% produces the lowest activation energy, which implies that the system has the greatest reactivity. This suggests that the most favorable BGE content in the epoxy healing system should be about 17.5%. For different BGE contents, the height of the peak for the first exothermic curve of each system is different, which indicates that BGE may have an impact on the curing reaction. On the other hand, there is not so much difference between the second exothermic peak of each system, which is basically very gentle. A likely explanation for this is that the curing agent MC120D is a microencapsulated latent curing agent. Accordingly, after the first peak, the wall of the curing agent MC120D is completely softened, which leads to the disappearance of the hysteresis

effect of the wall material on the curing reaction, thereby resulting in the consistent reactivity being shown by the system.

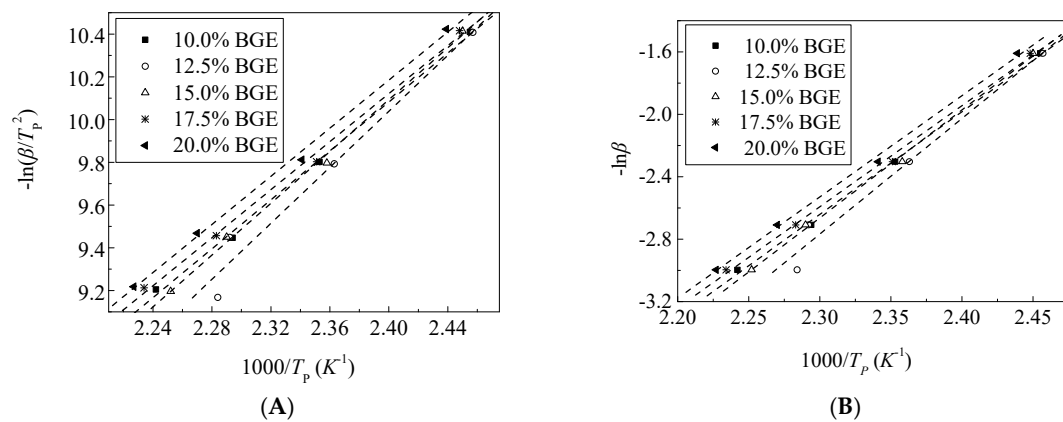


Figure 3. Linear fitting using the Kissinger equation and Crane equation. (A) $-\ln(\beta/T_p^2)$ vs. $1000/T_p$; (B) $-\ln\beta$ vs. $1000/T_p$.

Table 1. Activation energy and reaction order with different mass fractions of the diluent.

BGE Fraction (%)	$-\ln(\beta/T_p^2) \sim 1000/T_p$ Linear Fitting	Relative Coefficient R^2	Activation Energy E (kJ mol^{-1})	Reaction Order n
	$-\ln\beta \sim 1000/T_p$ Linear Fitting			
10.0	$y = -3.65469 + 5.72375x$ $y = -17.76639 + 6.57637x$	0.998 0.999	47.59	0.870
12.5	$y = -5.68331 + 6.55079x$ $y = -19.78786 + 7.40054x$	0.969 0.976	54.47	0.885
15.0	$y = -4.4576 + 6.06282x$ $y = -18.56654 + 6.91445x$	0.998 0.999	50.41	0.877
17.5	$y = -3.36634 + 5.61983x$ $y = -17.4921 + 6.47836x$	0.998 0.998	46.73	0.868
20.0	$y = -3.32175 + 5.62768x$ $y = -17.44446 + 6.48505x$	0.998 0.998	46.79	0.868

The reaction order n of the curing process is determined by the type of chemical reaction and the interaction of various reactions. The change in n should reflect the changes in the mechanism of the curing reaction. Thus, as the BGE content increases, basically, the reaction order of the curing process decreases. (See Table 1). This indicates that BGE is involved in the cross-linking of E-51. In addition, the curing reaction order of each system is less than one, indicating that the curing reaction is very complicated. Also, the finding that the values of the reaction order are relatively close indicates that there was no significant difference among the reactions of all the systems.

A comparison of the values of the frequency factor A (Table 2) of the respective heating rates at different BGE contents reveals that the value of A is relatively low when the BGE content is in the range of 17.5–20%. This indicates that this amount of BGE induced the largest resin curing degree. At this stage, the initial temperature and peak temperature are both relatively low. It can also be seen that the k value of each BGE content is not much different. Thus, the above system maintains the same activity at relatively low temperatures.

Table 2. Kinetic parameters of the curing reaction with different dosages of BGE.

BGE Fraction (%)	β (K·min ⁻¹)	T_i (K)	T_p (K)	T_f (K)	A (1/s)	k
10	5	347.3	407.3	447.3	2.19×10^5	0.17
	10	360.0	425.0	470.0	2.24×10^5	0.32
	15	366.0	436.0	481.0	2.27×10^5	0.45
	20	376.1	446.1	481.1	2.15×10^5	0.58
12.5	5	353.2	407.0	522.0	1.94×10^6	0.20
	10	363.2	423.2	533.2	1.93×10^6	0.37
	15	376.3	436.3	546.3	1.71×10^6	0.52
	20	352.8	437.8	552.8	2.16×10^6	0.68
15.0	5	348.0	408.2	448.2	5.13×10^5	0.18
	10	363.0	424.1	468.0	5.45×10^5	0.34
	15	361.7	436.7	476.7	5.10×10^5	0.48
	20	339.1	444.1	479.1	5.22×10^5	0.61
17.5	5	345.3	408.5	448.5	1.59×10^5	0.17
	10	363.1	425.3	470.3	1.70×10^5	0.31
	15	363.1	438.1	478.1	1.64×10^5	0.44
	20	372.7	447.7	482.7	1.59×10^5	0.56
20.0	5	355.0	410.0	450.0	1.53×10^5	0.17
	10	362.2	427.2	467.2	1.62×10^5	0.31
	15	365.6	440.6	480.6	1.53×10^5	0.43
	20	369.0	449.0	474.0	1.55×10^5	0.56

3.2. Effect of Curing Agent MC120D on Reaction Kinetics

The differential thermal curves of the system with the imidazole curing agent MC120D at a content of 10 to 50%, and a BGE content fixed at 17.5% are shown in Figure 4. The results that are shown in Figure 4, as well as those shown in Figure 2C, reveal that the differential thermal curves have two exothermic peaks for the MC120D content of 10% and 20%, whereas they have only one exothermic peak for the MC120D content of 30 to 50%. This finding indicates that the curing reaction of MC120D in a certain concentration range is a two-stage reaction. Once a certain amount is exceeded, the resin curing occurs in a one-step reaction. However, the reaction mechanism needs to be further studied. Like the situation for BGE, for different dosages of MC120D, as the heating rate increases, the initial temperature, peak temperature, and termination temperature also move toward the high temperature direction, and the higher the heating rate, the sharper the exothermic peak.

The results presented in Figure 5 show that the plots of $-\ln(\beta/T_p^2)$ vs. $1000/T_p$, and $-\ln\beta$ vs. $1000/T_p$ at different heating rates have a good linear relationship with the different amounts of MC120D, which findings are consistent with the kinetic analysis based on the Kissinger and Crane equations, respectively.

Like in the case of BGE, the activation energy and reaction order with different mass fractions of the catalyst, and the kinetic parameters of the curing reaction with different dosages of MC120D were obtained and they are shown in Tables 3 and 4. The data listed in Table 3 reveal that the activation energy reached its lowest value of 46.73 (kJ mol⁻¹) when the content of MC120D was 20%, indicating that the reactivity at this time reaches its maximum, which is consistent with the results presented in Table 1.

The data presented in Table 4, which were obtained by keeping the BGE content unchanged at 17.5%, show that the value of A for the MC120D content of 20% is much smaller than those for other MC120D contents under different heating rates. This finding indicates that the curing performance of the epoxy resin system reaches its best performance under this condition, which is consistent with the above results.

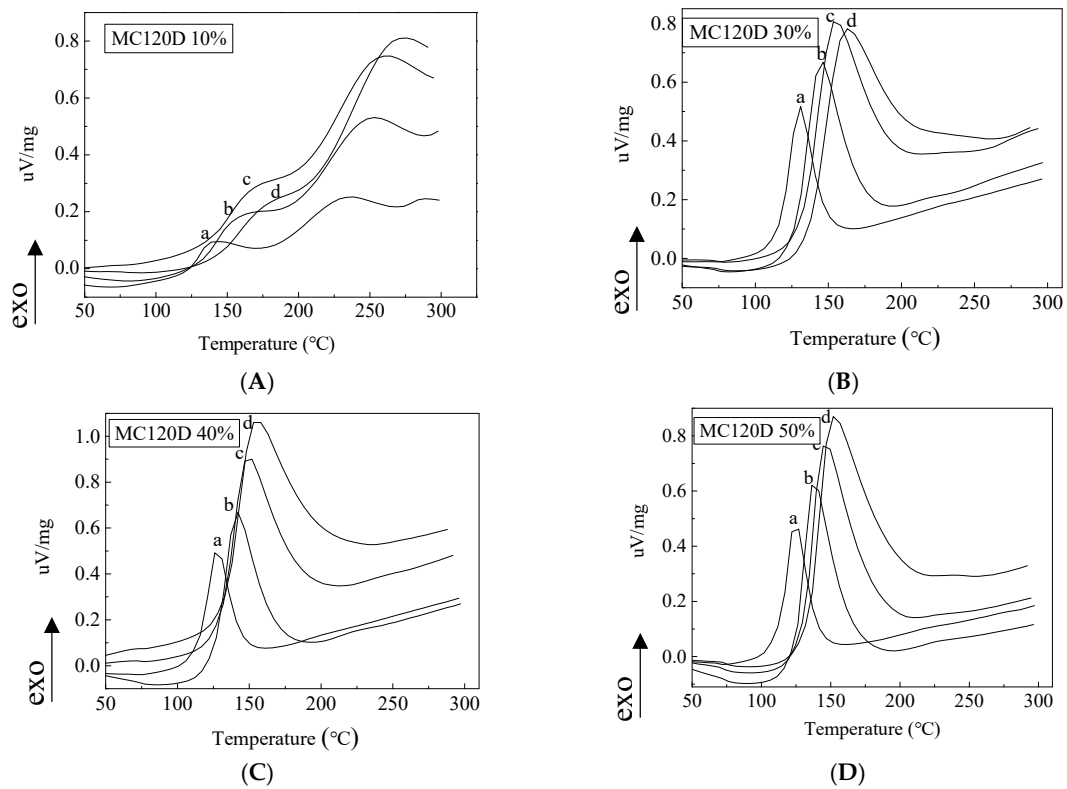


Figure 4. Differential thermal analysis of the healing system with different mass fractions of MC120D (a. 5 K/min, b. 10 K/min, c. 15 K/min, d. 20 K/min). (A) 10% MC120D; (B) 30%; (C) 40%; and (D) 50%.

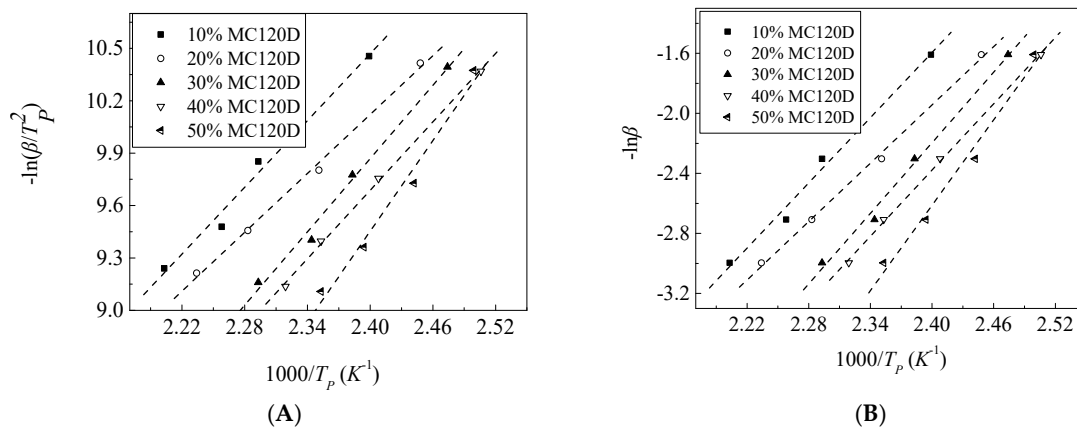


Figure 5. Linear fitting using the Kissinger equation and Crane equation. (A) $-\ln(\beta/T_p^2)$ vs. $1000/T_p$; (B) $-\ln\beta$ vs. $1000/T_p$.

In the previous tests, the components of the core healing agent and curing agent were investigated. Whereas the microcapsule itself has not been involved, although the self-healing function is realized by the microcapsules. The average diameter of the synthesized microcapsules is from 100 μm to 500 μm . The thickness of the microcapsule wall is about 10 μm . Regarding the size of microcapsule, it may have influence on both the synthesis of microcapsules and the curing reaction. the kinetics of synthesis of UF microcapsules can refer to Ref. [33], while for the curing reaction, the size of a microcapsule provides different content of core agent. In view of the volume of a microcapsule, the core content is proportional to the third power of the diameter minus the wall thickness. For the situation of microcapsules embedded in cementitious materials, the behavior is much more complicated and needs further research.

Table 3. Activation energy and reaction order with different mass fractions of the catalyst.

MC120D Fraction (%)	$-\ln(\beta/T_p^2) \sim 1000/T_p$ Linear Fitting	Relative Coefficient R^2	Activation Energy E (kJ mol ⁻¹)	Reaction Order n
	$-\ln\beta \sim 1000/T_p$ Linear Fitting			
10	$y = -4.81416 + 6.36782x$	0.985	52.94	0.880
	$y = -18.96889 + 7.23911x$	0.989		
20	$y = -3.36634 + 5.61983x$	0.998	46.73	0.868
	$y = -17.4921 + 6.47836x$	0.998		
30	$y = -6.91955 + 6.99507x$	0.991	58.16	0.892
	$y = -21.00677 + 7.83769x$	0.993		
40	$y = -5.98578 + 6.53037x$	0.999	54.30	0.888
	$y = -20.03786 + 7.35817x$	0.999		
50	$y = -11.31952 + 8.65504x$	0.981	71.96	0.913
	$y = -25.37057 + 9.48248x$	0.984		

Table 4. Kinetic parameters of curing reaction with different dosages of MC120D.

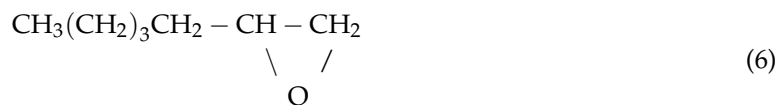
MC120D Fraction (%)	β (K·min ⁻¹)	T_i (K)	T_p (K)	T_f (K)	A (1/s)	k
10	5	351.9	416.9	446.9	7.87×10^5	0.18
	10	356.1	436.1	456.1	7.35×10^5	0.33
	15	367.9	442.9	467.9	8.53×10^5	0.49
	20	378.9	453.9	478.9	7.65×10^5	0.62
20	5	345.3	408.5	448.5	1.59×10^5	0.17
	10	363.1	425.3	470.3	1.70×10^5	0.31
	15	363.1	438.1	478.1	1.64×10^5	0.44
	20	372.7	447.7	482.7	1.59×10^5	0.56
30	5	346.6	404.2	439.2	7.02×10^6	0.21
	10	361.1	419.6	469.6	6.90×10^6	0.40
	15	371.1	426.6	486.6	7.63×10^6	0.58
	20	376.1	436.1	526.1	6.80×10^6	0.74
40	5	344.1	399.1	434.1	2.62×10^6	0.20
	10	370.3	415.3	470.3	2.56×10^6	0.38
	15	355.0	425.0	485.0	2.55×10^6	0.54
	20	371.1	431.1	511.1	2.66×10^6	0.70
50	5	350.0	400.1	430.1	6.70×10^8	0.27
	10	364.5	409.5	464.5	7.77×10^8	0.52
	15	362.7	417.7	482.7	7.41×10^8	0.74
	20	375.0	425.0	495.0	6.69×10^8	0.96

3.3. Curing Reaction Mechanism for the Healing Agent

In the previous section, it was revealed that when the MC120D content was 20% and the BGE content was 12.5~20%, there were two exothermic peaks at around 150 and 250 °C, respectively. When the BGE content was 17.5%, and the MC120D content was 10% and 20%, there were two exothermic peaks, near 150 and 250 °C, respectively. Instead, there was only one exothermic peak at about 150 °C when the content was over 30%. In order to further elucidate the mechanism of the differential thermal profile of each component, the epoxy resin cured product was analyzed.

The infrared spectrum of epoxy resin E-51 displayed in Figure 6A reveals the presence of the absorption peaks at 771 cm⁻¹ for epoxy, at 1184 cm⁻¹ for C-N stretching vibration, at 1247 and 1035 cm⁻¹ for ether bond stretching vibrations, at 1361 cm⁻¹ for the bismuth symmetric vibration of bisphenol A, at 1508, 1583, 1607, and 831 cm⁻¹ for the vibrations of the benzene ring, at 2869 cm⁻¹ for the methylene stretching vibration, at 2928 cm⁻¹ for the C-H stretching vibration in CH₂, at 2967 cm⁻¹ for the C-H antisymmetric stretching vibration peak in CH₃ and at 3482 cm⁻¹ for the hydroxyl group [34].

The FTIR spectrum of diluent BGE is displayed in Figure 6B. The structure of BGE [35] is shown below.



The absorption peak at 1110 cm^{-1} was generated by the stretching vibration of the linear fatty ether structure. The peaks at 913 , 844 , and 761 cm^{-1} are the vibration absorptions of the epoxy ring. Among them, the peak at 913 cm^{-1} is an end-epoxy type absorption peak. The change in these peaks can be used to determine the extent to which the ring opening reaction proceeds. Among the three absorption bands, the one at 844 cm^{-1} has the strongest absorption and it is generated by the antisymmetric stretching vibration of the epoxy ring [36].

The FTIR spectra of the cured products of the epoxy resin are shown in Figure 7. The composition of the healing agent is as follows: MC120D content is 20% of the epoxy resin E-51 mass, and diluent BGE content is 12.5% (curve c in Figure 7A), 15% (curve d in Figure 7A), and 20% (curve e in Figure 7A) of the epoxy resin E-51 mass.

The curing temperatures in Figure 7 encompass the first exothermic peak temperature range of the differential thermal profile of the epoxy resin in Figure 2. The FTIR curves of the different BGE contents reveal that the main characteristic absorption peaks of epoxy resin E-51 at 771 cm^{-1} , 1035 cm^{-1} , 1184 cm^{-1} , 1361 cm^{-1} , and 2928 cm^{-1} disappeared, but the peak at 1607 cm^{-1} did not change much. These results indicate that the heat resistance of the functional group is good, and it did not react at that temperature. Meanwhile, the epoxy spectra absorption peaks of BGE at 913 , 844 , and 761 cm^{-1} also disappeared, which demonstrated that the epoxy ring fully participated in the curing reaction [37]. The data presented in Figure 7B show that the strength at 3482 cm^{-1} increases with the increase in the BGE content, which indicates that the polymerization reaction produces new hydroxyls.

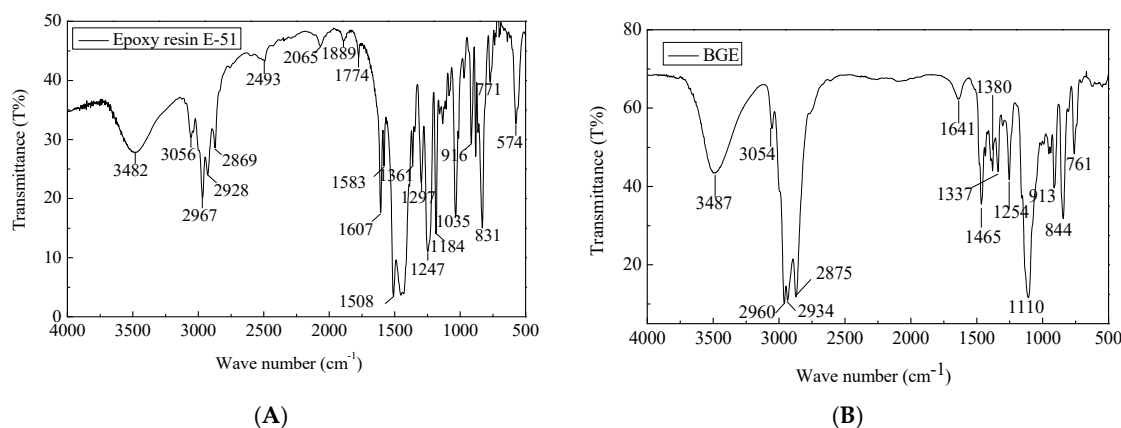


Figure 6. Fourier-transform infrared spectroscopy (FTIR) spectra of the healing agent. (A) the epoxy resin E-51; (B) the diluent BGE.

The FTIR spectra of the same samples as those shown in Figure 7 are displayed in Figure 8. However, the temperature was raised to $270 \text{ }^\circ\text{C}$, which encompasses the temperature range of the second exothermic peak of the differential thermal curves shown in Figure 2 for the epoxy resin curing reaction. The spectra reveal that the changes for the main characteristic peaks of the epoxy resin E-51 and BGE are similar to those that are presented in Figure 7. In Figure 7B, the red, blue and pink represent b(E-51 + 12.5%BGE), c(E-51 + 15%BGE), and d(E-51 + 20%BGE), respectively.

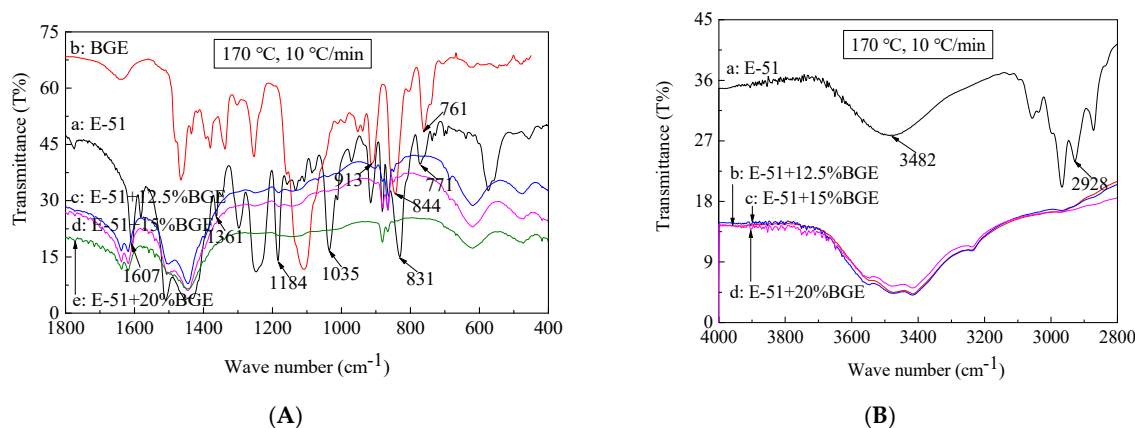


Figure 7. FTIR spectra of the cured epoxy resin at 170 °C (20% MC120D). (A) E-51; (B) Hydroxyl peak of cured bisphenol A diglycidyl ether (BADGE).

The data presented in Figures 7 and 8 show not only that the epoxy resin E-51 was cured, but also that the BGE was involved in the cross-linking reaction of the epoxy resin E-51 with MC120D. The curing mechanism in the formation of the terpolymer is [38,39], as follows: The tertiary amine with lone pair electrons on the imidazole ring underwent an addition reaction with the epoxide and generated an adduct. The reaction of the adduct with another epoxy produced a complex with both positive and negative ions coexisting in the molecule. The negative ions in the complex are the active sites and can catalyze the co-condensation reaction of the epoxy groups to produce terpolymers of epoxy resins, diluents, and imidazole, as shown in Figure 9.

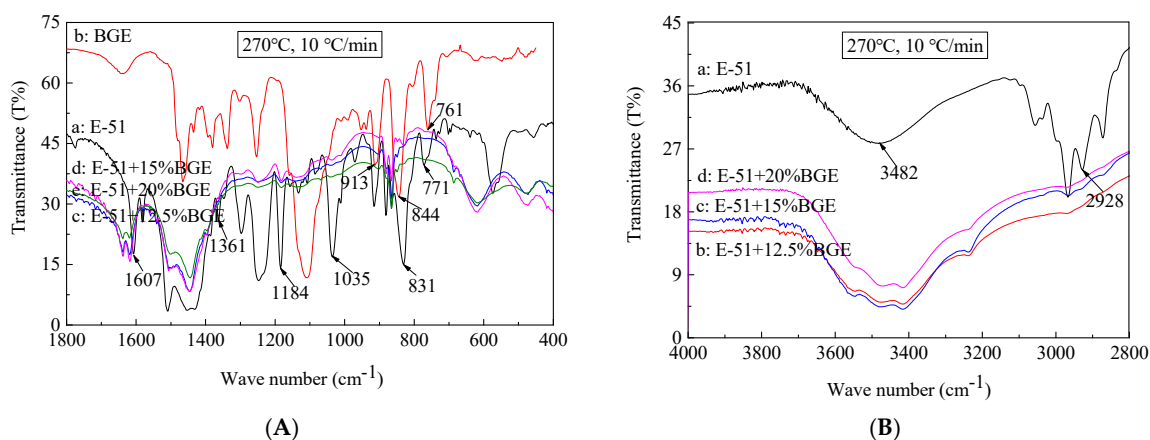


Figure 8. FTIR spectra of the cured epoxy resin at 270 °C (20% MC120D). (A) E-51; (B) Hydroxyl peak of cured bisphenol A diglycidyl ether (BADGE).

The FTIR spectra of the cured product with the content of the curing agent MC120D and the diluent BGE both at 20% the mass of the epoxy resin are shown in Figure 10A. The temperature was increased from room temperature to either 170 °C or 270 °C, at a heating rate of 10 °C/min. The spectra reveal that at the maximum temperature from 170 °C to 270 °C, the -OH characteristic peak at 2331 cm⁻¹, and the CH characteristic peak at 2360 cm⁻¹ disappeared. This explains why the second exothermic peak exists in the differential thermal curve in Figure 2.

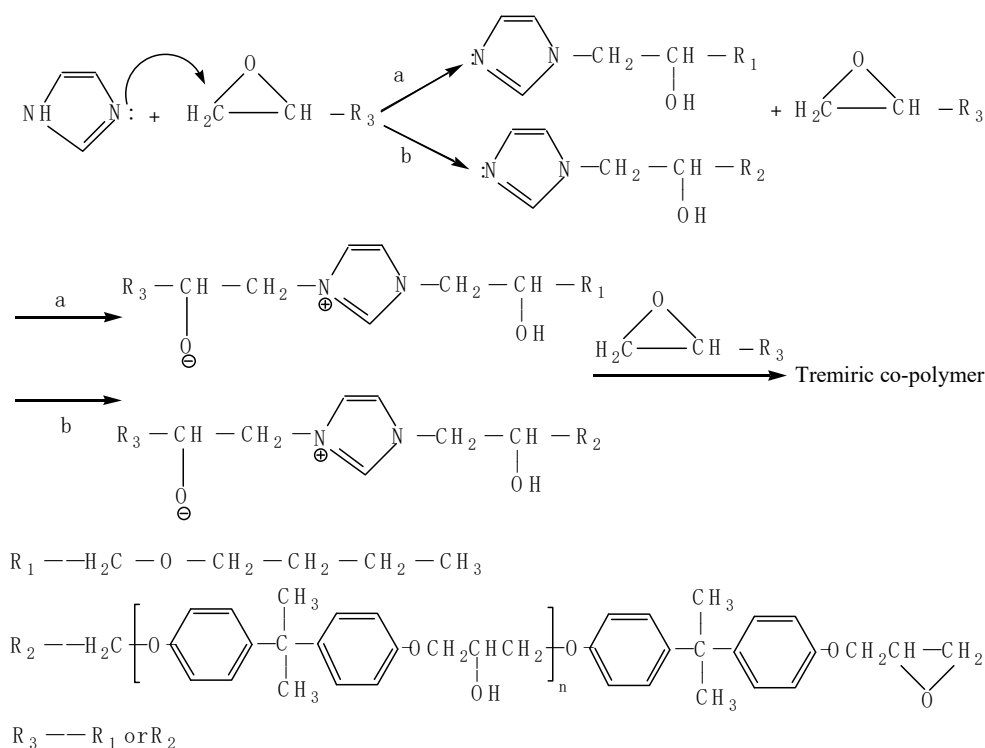


Figure 9. Curing reaction of the E-51/BGE/MC120D system.

The FTIR spectra of the cured product with a BGE content of 17.5% of the epoxy resin E-51 and a MC120D content of either 10% or 40% are shown in Figure 10B. The temperature was increased from room temperature to 170 °C at a heating rate of 10 °C /min. The spectrum of the cured product when the content of MC120D is 10% shows two characteristic peaks, one corresponds to the vibration peak of the benzene ring at 1500 cm^{-1} and the other is the stretching vibration peak of C=O at 1641 cm^{-1} . However, when the content of MC120D is 40%, these two characteristic peaks disappear.

According to the previous section and the data presented in Figure 10A,B, the peaks at 1500 and 1641 cm^{-1} both exist in the two curves of 170 °C and 270 °C, indicating that the two groups in the system had good heat resistance. Indeed, when the MC120D content is less than 20%, it will not be significantly changed, even at a high temperature. However, when the amount of MC120D exceeds 30%, the two groups are involved in the reaction under the action of sufficient catalyst, and the characteristic peaks disappear, so that there is only one exothermic peak on the differential thermal curve.

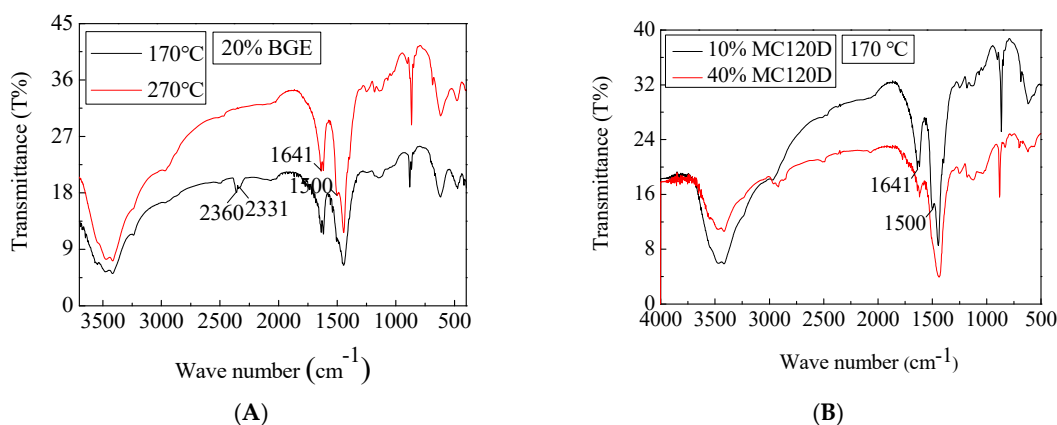


Figure 10. Hydroxyl peak of the cured BADGE resin. (A) 20% MC120D; (B) 17.5% BGE. Absorption peak of epoxy resin cured product.

4. Conclusions

In this study, the crosslinking and curing reaction kinetics of the healing agent were analyzed. The effect of diluent BGE was investigated for five mass fractions of 10.0%, 12.5%, 15.0%, 17.5%, and 20.0% BGE to epoxy resin. Using the Kissinger and Crane equations, the activation energy and reaction order with different diluent mass fractions, as well as the kinetic parameters of the curing reaction, were determined. The optimal fraction of BGE was determined to be 17.5%. In addition, the effect of the curing agent MC120D on the reaction kinetics was investigated for 10%, 20%, 30%, 40%, and 50% mass fractions of MC120D to epoxy resin, and the optimal mass fraction of MC120D was determined to be 20%. As it was realized that the curing reaction involved in the system of epoxy resin E-51, diluent BGE and curing agent MC120D is a complex reaction, the mechanism of the curing reaction for the healing agent was investigated. The infrared spectra of the cured product with different fractions of the healing agent were analyzed and the mechanism of appearance and disappearance of the exothermic peaks was determined. In this study, only the curing reaction was considered. The findings of this study should benefit the design of the mix proportion of the microcapsule-based self-healing system.

In future research, it is necessary to further investigate the interface between the cured product of the healing agent and the cementitious matrix, as well as the mechanism of movement of the healing agent on the crack surfaces.

Author Contributions: Conceptualization (F.X. and N.H.); data curation (M.Z. and X.W.); funding acquisition (F.X. and X.W.); investigation (M.Z.); supervision (F.X., N.H. and X.W.); writing, original draft (M.Z. and X.W.); writing, review and editing (X.W. and N.H.).

Funding: This research was funded by the National Natural Science Foundation of China, grant number 51478272; the joint funds of the National Natural Science Foundation and Guangdong Province of China, grant number U1301241; the Science and Technology Foundation of Shenzhen City, grant number JCYJ20160422095146121; and the Collaborative Innovation Research Centre for Environment-Friendly Materials and Structures in Civil Engineering, Southeast University.

Conflicts of Interest: The authors declare no conflict of interest.

References

1. Mihashi, H.; Nishiwaki, T. Development of engineered self-healing and self-repairing concrete-state-of-the-art report. *J. Adv. Concr. Technol.* **2012**, *10*, 170–184. [[CrossRef](#)]
2. Van Tittelboom, K.; De Belie, N. Self-healing in cementitious materials—A review. *Materials* **2013**, *6*, 2182–2217. [[CrossRef](#)] [[PubMed](#)]
3. Tang, W.C.; Kardani, O.; Cui, H.Z. Robust evaluation of self-healing efficiency in cementitious materials—A review. *Constr. Build. Mater.* **2015**, *81*, 233–247. [[CrossRef](#)]
4. Souradeep, G.; Kua, H. Encapsulation technology and techniques in self-healing concrete. *J. Mater. Civ. Eng.* **2016**, *28*. [[CrossRef](#)]
5. Liu, Q.; Li, B.; Schlangen, E.; Sun, Y.; Wu, S. Research on the mechanical, thermal, induction heating and healing properties of steel slag/steel fibers composite asphalt mixture. *Appl. Sci.* **2017**, *7*, 1088. [[CrossRef](#)]
6. Tabaković, A.; Schuyffel, L.; Karač, A.; Schlangen, E. An evaluation of the efficiency of compartmented alginate fibres encapsulating a rejuvenator as an asphalt pavement healing system. *Appl. Sci.* **2017**, *7*, 647. [[CrossRef](#)]
7. Cuenca, E.; Tejedor, A.; Ferrara, L. A methodology to assess crack-sealing effectiveness of crystalline admixtures under repeated cracking-healing cycles. *Constr. Build. Mater.* **2018**, *179*, 619–632. [[CrossRef](#)]
8. Wang, X.F.; Xing, F.; Zhang, M.; Han, N.X.; Qian, Z.W. Experimental study on cementitious composites embedded with organic microcapsules. *Materials* **2013**, *6*, 4064–4081. [[CrossRef](#)] [[PubMed](#)]
9. Wang, X.F.; Xing, F.; Xie, Q.; Han, N.X.; Kishi, T.; Ahn, T.H. Mechanical behavior of a capsule embedded in cementitious matrix-macro model and numerical simulation. *J. Ceram. Process. Res.* **2015**, *16*, 74–82.
10. Wang, X.; Sun, P.; Han, N.; Xing, F. Experimental study on mechanical properties and porosity of organic microcapsules based self-healing cementitious composite. *Materials* **2017**, *10*, 20. [[CrossRef](#)] [[PubMed](#)]

11. Wang, X.F.; Han, R.; Han, T.L.; Han, N.X.; Xing, F. Determination of elastic properties of urea-formaldehyde microcapsules through nanoindentation based on the contact model and the shell deformation theory. *Mater. Chem. Phys.* **2018**, *215*, 346–354. [[CrossRef](#)]
12. Wang, X.F.; Han, R.; Tao, J.; Han, T.L.; Zhu, G.M.; Tang, J.N.; Han, N.X.; Xing, F. Identification of mechanical parameters of urea-formaldehyde microcapsules using finite-element method. *Compos. Part B Eng.* **2018**, *158*, 249–258. [[CrossRef](#)]
13. Han, N.; Xing, F. Intelligent resilience of cementitious materials for marine infrastructures. *J. Ceram. Process. Res.* **2015**, *16*, 14–21.
14. Han, N.-X.; Xing, F. A comprehensive review of the study and development of microcapsule based self-resilience systems for concrete structures at Shenzhen University. *Materials* **2017**, *10*, 2. [[CrossRef](#)] [[PubMed](#)]
15. Zhang, M. A Study on Microcapsule Based Self-Healing Method and Mechanism for Cementitious Composites. Ph.D. Thesis, Central South University, Changsha, China, 30 May 2013.
16. Al-Mansoori, T.; Norambuena-Contreras, J.; Garcia, A. Effect of capsule addition and healing temperature on the self-healing potential of asphalt mixtures. *Mater. Struct.* **2018**, *51*, 53. [[CrossRef](#)]
17. Su, J.-F.; Schlangen, E.; Qiu, J. Design and construction of microcapsules containing rejuvenator for asphalt. *Powder Technol.* **2013**, *235*, 563–571. [[CrossRef](#)]
18. Su, J.-F.; Yang, P.; Wang, Y.-Y.; Han, S.; Han, N.-X.; Li, W. Investigation of the self-healing behaviors of microcapsules/bitumen composites by a repetitive direct tension test. *Materials* **2016**, *9*, 600. [[CrossRef](#)] [[PubMed](#)]
19. Su, J.-F.; Wang, Y.-Y.; Han, N.-X.; Yang, P.; Han, S. Experimental investigation and mechanism analysis of novel multi-self-healing behaviors of bitumen using microcapsules containing rejuvenator. *Constr. Build. Mater.* **2016**, *106*, 317–329. [[CrossRef](#)]
20. Lv, L.; Yang, Z.; Chen, G.; Zhu, G.; Han, N.; Schlangen, E.; Xing, F. Synthesis and characterization of a new polymeric microcapsule and feasibility investigation in self-healing cementitious materials. *Constr. Build. Mater.* **2016**, *105*, 487–495. [[CrossRef](#)]
21. Lv, L.; Schlangen, E.; Yang, Z.; Xing, F. Micromechanical properties of a new polymeric microcapsule for self-healing cementitious materials. *Materials* **2016**, *9*, 1025. [[CrossRef](#)] [[PubMed](#)]
22. Wang, J.Y.; Soens, H.; Verstraete, W.; De Belie, N. Self-healing concrete by use of microencapsulated bacterial spores. *Cem. Concr. Res.* **2014**, *56*, 139–152. [[CrossRef](#)]
23. Van Stappen, J.; Bultreys, T.; Gilbert, F.A.; Hillewaere, X.K.D.; Gómez, D.G.; Van Tittelboom, K.; Dhaene, J.; De Belie, N.; Van Paepegem, W.; Du Prez, F.E. The microstructure of capsule containing self-healing materials: A micro-computed tomography study. *Mater. Charact.* **2016**, *119*, 99–109. [[CrossRef](#)]
24. Šavija, B.; Feiteira, J.; Araújo, M.; Chatrabhuti, S.; Raquez, J.-M.; Van Tittelboom, K.; Gruyaert, E.; De Belie, N.; Schlangen, E. Simulation-aided design of tubular polymeric capsules for self-healing concrete. *Materials* **2017**, *10*, 10. [[CrossRef](#)] [[PubMed](#)]
25. Paluvai, N.R.; Mohanty, S.; Nayak, S.K. Synthesis and modifications of epoxy resins and their composites: A review. *Polym. Plast. Technol. Eng.* **2014**, *53*, 1723–1758. [[CrossRef](#)]
26. Pane, I.; Hansen, W. Investigation of blended cement hydration by isothermal calorimetry and thermal analysis. *Cem. Concr. Res.* **2005**, *35*, 1155–1164. [[CrossRef](#)]
27. Yuan, Y.C.; Rong, M.Z.; Zhang, M.Q. Preparation and characterization of microencapsulated polythiol. *Polymer* **2008**, *49*, 2531–2541. [[CrossRef](#)]
28. Kissinger, H.E. Reaction Kinetics in differential thermal analysis. *Anal. Chem.* **1957**, *29*, 1702–1706. [[CrossRef](#)]
29. Crane, L.W.; Dynes, P.J.; Kaelble, D.H. Analysis of curing kinetics in polymer composites. *J. Polym. Sci.* **1973**, *11*, 533–538. [[CrossRef](#)]
30. Choi, E.J.; Seo, J.C.; Bae, H.-K.; Lee, J.K. Synthesis and curing of new aromatic azomethine epoxies with alkoxy side groups. *Eur. Polym. J.* **2004**, *40*, 259–265. [[CrossRef](#)]
31. Farkas, A.; Strohm, P.F. Imidazole catalysis in the curing of epoxy resins. *J. Appl. Polym. Sci.* **1968**, *12*, 159–168. [[CrossRef](#)]
32. Ricciardi, F.; Romanchick, W.A.; Joullie, M.M. 1,3-dialkylimidazolium salts as latent catalysts in the curing of epoxy resins. *J. Polym. Sci. Polym. Lett. Ed.* **1983**, *21*, 1475–1481. [[CrossRef](#)]
33. Ni, Z.; Du, X.X.; Wang, S.; Xing, F. Kinetics of synthesis of UF microcapsules. *J. Shenzhen Univ. Sci. Eng.* **2011**, *28*, 249–254.

34. González, M.G.; Cabanelas, J.C.; Baselga, J. *Applications of FTIR on Epoxy Resins—Identification, Monitoring the Curing Process, Phase Separation and Water Uptake, Infrared Spectroscopy—Materials Science, Engineering and Technology*; Theophile, T., Ed.; IntechOpen Limited: London, UK, 2012; pp. 261–284. ISBN 978-953-51-0537-4.
35. Parameswaranpillai, J.; Hameed, N.; Pionteck, J.; Woo, E.M. *Handbook of Epoxy Blends*; Springer: Cham, Switzerland, 2017; ISBN 978-3-319-40041-9.
36. Panda, H. *Epoxy Resins Technology Handbook (Manufacturing Process, Synthesis, Epoxy Resin Adhesives and Epoxy Coatings)*; Asia Pacific Business Press Inc.: Delhi, India, 2017; ISBN 978-8178331744.
37. Abdelkader, A.F.; White, J.R. Curing characteristics and internal stresses in epoxy coatings: Effect of crosslinking agent. *J. Mater. Sci.* **2005**, *40*, 1843–1854. [[CrossRef](#)]
38. Ooi, S.K.; Cook, W.D.; Simon, G.P.; Such, C.H. DSC studies of the curing mechanisms and kinetics of BADGE using imidazole curing agents. *Polymer* **2000**, *41*, 3639–3649. [[CrossRef](#)]
39. Du, X.X. Self-Healing Microcapsules and Its Polymer Composite Materials. Master's Thesis, Shenzhen University, Shenzhen, China, 1 June 2009.



© 2018 by the authors. Licensee MDPI, Basel, Switzerland. This article is an open access article distributed under the terms and conditions of the Creative Commons Attribution (CC BY) license (<http://creativecommons.org/licenses/by/4.0/>).